Statistically bias-corrected and downscaled climate models underestimate the severity of U.S. maize yield shocks

Supplementary Information

NEX-GDDP Climate Data. The NASA NEX-GDDP technical note can be found at:

https://esgf.nccs.nasa.gov/esgdoc/NEX-GDDP_Tech_Note_v0.pdf

The Technical Note contains a detailed description of the separate algorithms used to downscale and bias-correct the raw CMIP5 model outputs. Here we describe only the central steps.

The bias-correction procedure performs a quantile-mapping in which for each variable, a transfer function is applied to the GCM-generated cumulative distribution function (CDF) such that the quantiles are set to align with observational data. CDFs are constructed for each day of the year by pooling the target day $\pm$15 days over the entire historical period, 1950-2005. This corrects the statistical moments of the GCM output. The downscaling or spatial disaggregation step performs a scaled bilinear interpolation of the GCM-generated fields that respects the monthly climatology of the observational data. Both steps are implemented such that the monthly trends (specifically, the 9-year running average for each month) in the GCM outputs remain unchanged. These approaches assume stationarity: the spatial patterns of the mapping functions derived from the historical time period are assumed to remain the same in the future.

The observational/reanalysis product that was used to perform both the bias-correction and downscaling is the Global Meteorological Forcing Dataset (GMFD;[1]). GMFD was developed to provide near-surface meteorological variables, derived via a globally consistent methodology, suitable for forcing models of land surface processes. It was produced by combining multiple global observational products with the NCEP/NCAR Reanalysis dataset.

Skill of climate variables. There are two broad classes of models available to simulate agricultural yields: process-based[2] and statistical[3]. Process-based models explicitly simulate the physiological mechanisms of plant growth. They typically require extensive

calibration for a large number of inputs, including soil information, solar radiation data, and farm management decisions like planting/harvesting dates and fertilizer application practices. In contrast, statistical models employ regression techniques to predict agricultural outcomes from fine-scale weather data. They benefit from increasingly large and detailed datasets and can implicitly account for farm management decisions. Although methodologically somewhat different, a recent study finds that both approaches give very similar predictions when compared over the same region, particularly when the effects of carbon dioxide are neglected[4]. Innovative new machine-learning approaches, such as random forests[5–7] and neural networks[8], have also shown considerable skill in reproducing historical yields.

Here, we adapt a statistical model originating from Schlenker and Roberts[9]. This statistical model is more parsimonious and transparent than process-based models and it readily allows us to predict yield variations based solely on NEX-GDDP output variables.

As described in the main text, our yield model is given by:

$$\log Y_{i,t} = f_i(t) \; + \; c_i + \alpha_i \, GDD'_{i,t} + \beta_i \, EDD'_{i,t} + \gamma_i \, P'_{i,t} + \kappa_i \, {P'_{i,t}}^2 \; + \; \epsilon_{i,t} \; . \qquad (1)$$

We implement a test to check whether the above model is an improvement over the sub-model of describing yields by the technological time trend only, given by

$$\log Y_{i,t} = f_i(t) \; + \; \epsilon_{i,t}. \qquad (2)$$

This test is to ensure that in the main text, our conclusions are drawn from counties where including climatic variables in the yield model is meaningful in the sense of providing additional skill. An argument could be made that if the fit is worsened by the inclusion of climate data, any uncertainty analysis surrounding that data would be rendered irrelevant. In order to guard against this, in the main text we include only counties where Eq. (1) provides a lower mean squared error than Eq. (2) measured via leave-one-out cross-validation.

Counties for which the full model gives a worse fit are shown in red in Figure S13, and counties for which the full model gives a better fit are shown in green. The boundary is predominantly north-south oriented and approximately traces the 100W meridian, which previous studies[9–11] have used as a first-order boundary between irrigated maize (to the west) and rainfed maize (to the east). Irrigated crops are generally less sensitive to fluctuations in weather and thus less well-suited to regression analysis, a result that emerges qualitatively here.

62 Our quantitative results are very similar if all counties are included (Figures S7, S8,
63 S9), reflecting that most of the historically high-production counties are better modeled via
64 Eq. (1). For all years throughout the historical time period, counties better modeled by Eq.
65 (1) accounted for no less than 80% of the national production share (Figure S11).
66

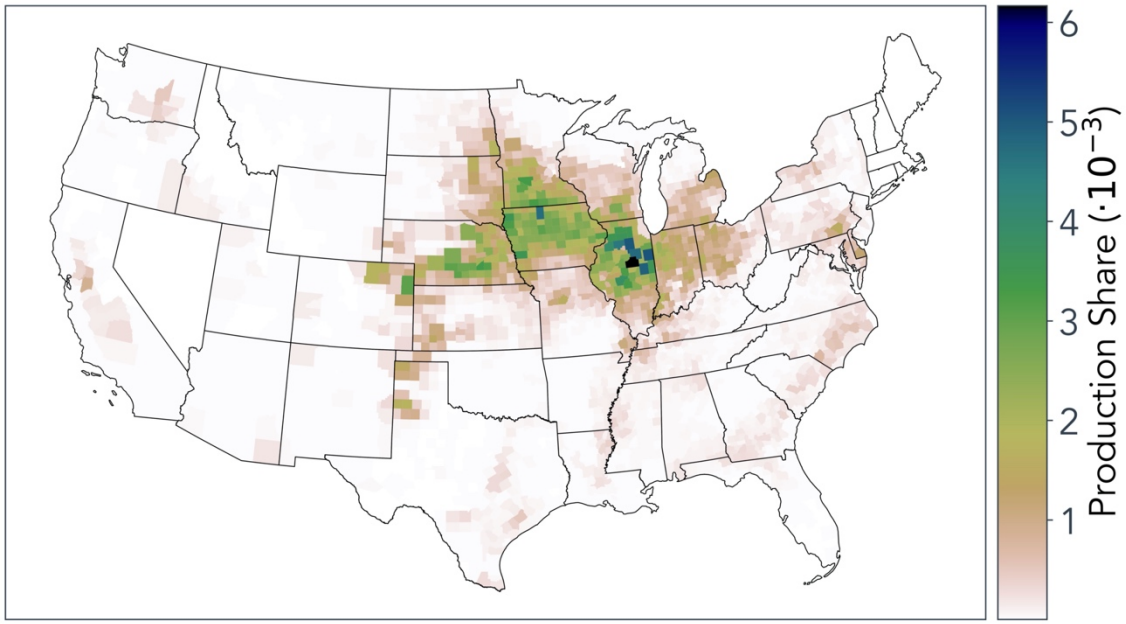

Fig. S1. 1960-2016 mean county production shares. Note that in the main text, for all analysis over the historical period we use yearly production shares. The averages are used in the projections and can give an idea of which counties have been historically important.

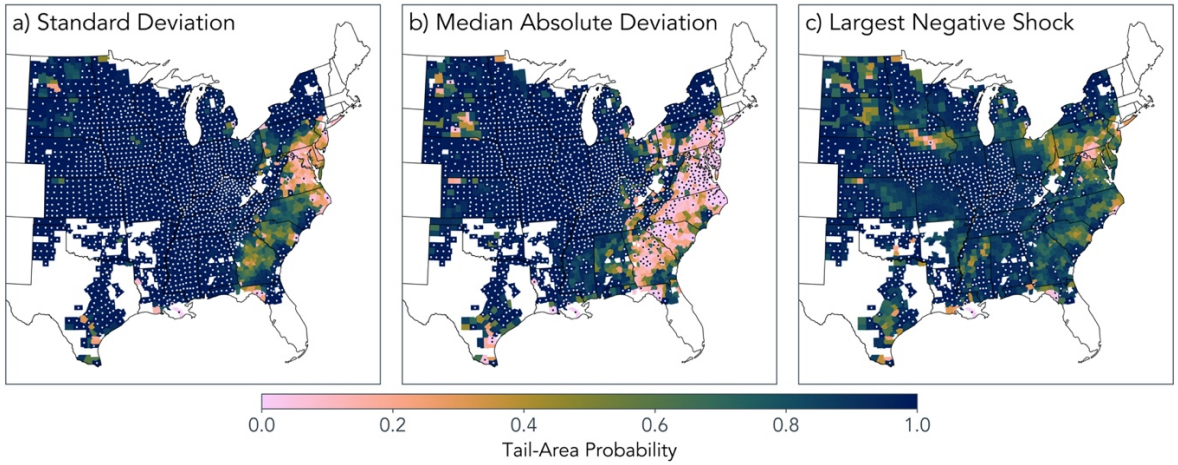

Figure S2. Tail-area probabilities of CMIP-modeled maize yields measured against observationally driven yields. Results are shown for standard deviation (a), median absolute deviation (b), and the magnitude of the largest negative yield shock (c). Stippling indicates tail-area probabilities less than 0.01 or greater than 0.99.

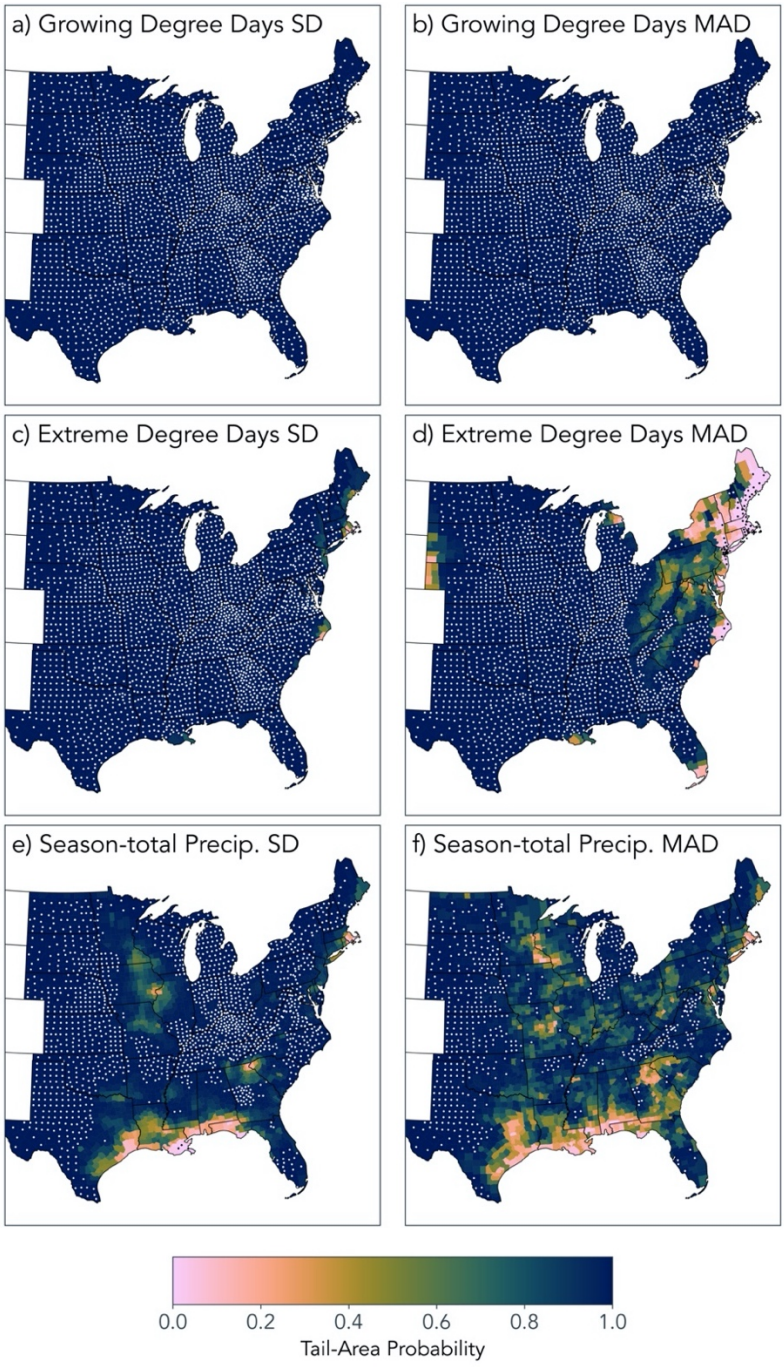

77

78 **Figure S3.** Tail-area probabilities for each climate variable in the yield model, from the CMIP
79 ensemble. The left column shows standard deviation; the right column median absolute deviation
80 (MAD). Climate variables are organized by row: growing degree days (top), extreme degree days
81 (middle), precipitation (bottom). Stippling indicates tail-area probabilities less than 0.01 or greater
82 than 0.99.

83

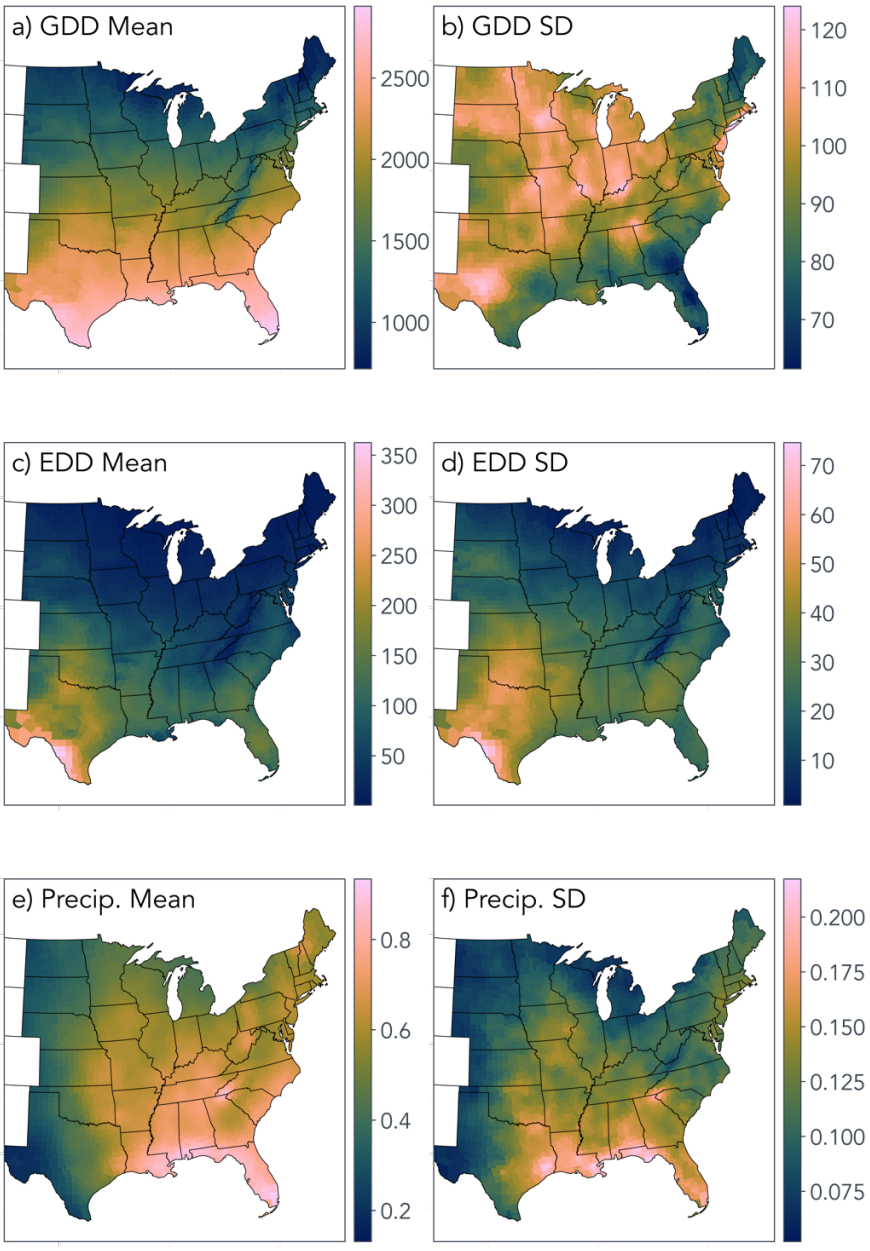

Figure S4. Historical mean and standard deviation for each climate variable in the yield model, calculated from the reanalysis. The left column shows the mean; the right column standard deviation (SD). Climate variables are organized by row: growing degree days (top), extreme degree days (middle), precipitation (bottom).

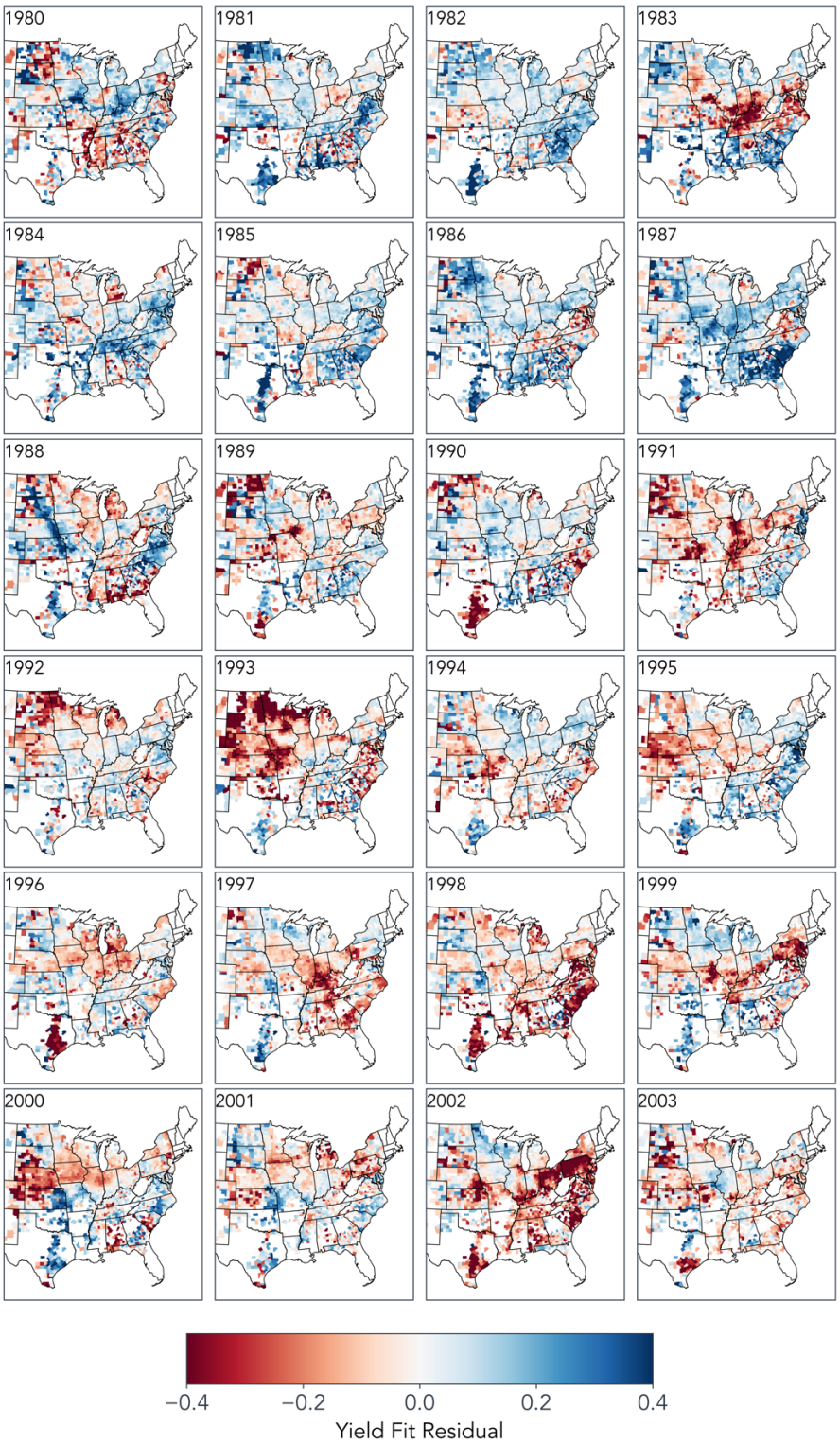

Figure S5. Yield model fit residuals for 24 consecutive years during the historical time period, showing considerable spatial correlation.

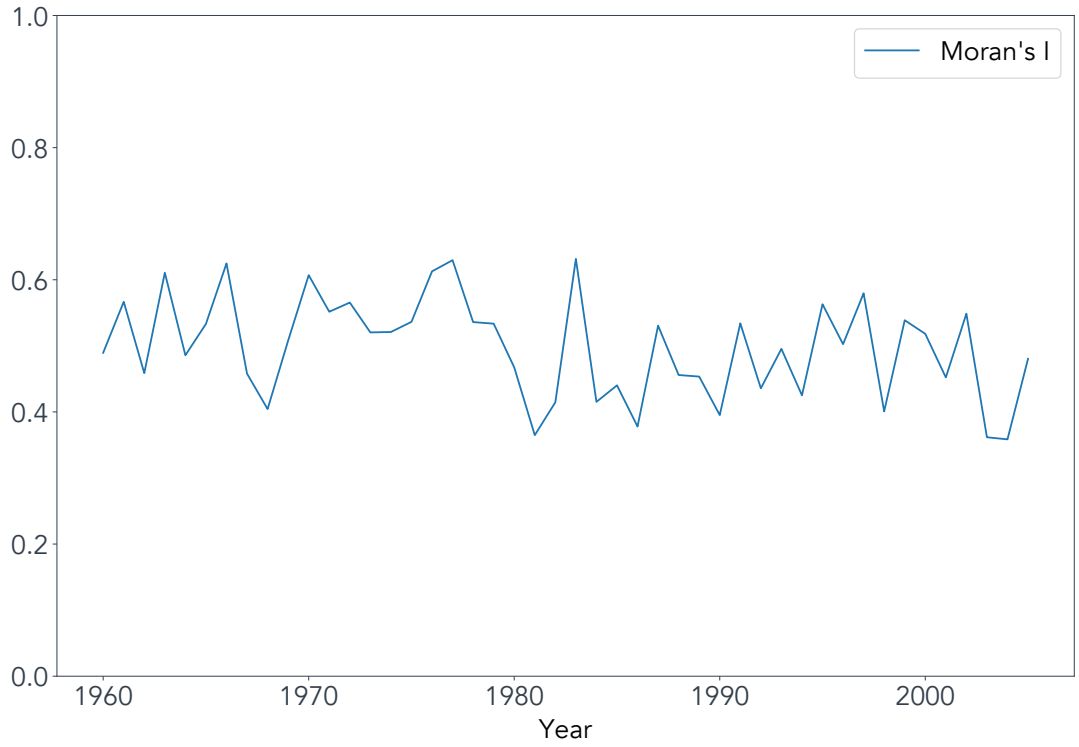

Figure S6. Moran's I, a measure of global spatial autocorrelation, over the entire historical period. A k-nearest-neighbors algorithm with *k=10* is used to calculate the spatial weights matrix, using only the counties that show improved skill after including the climate variables. Values close to 1 indicate highly correlated data. The null hypothesis of spatial independence, a hypothesis that we made in the main text, can be rejected for all years ($P < 0.001$).

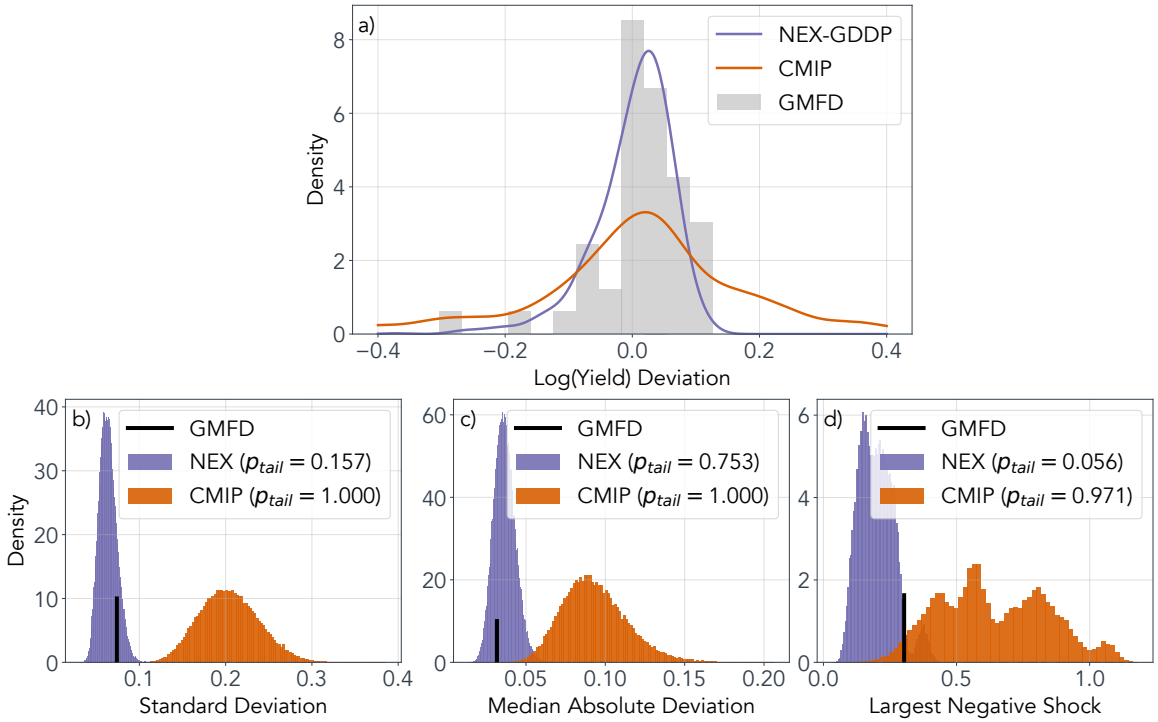

100

101 **Figure S7.** As Figure 1 in the main text but including all counties, regardless of whether including
102 climate variables increases skill. Tail-area probabilities for the CMIP ensemble differ only at the
103 third decimal place. Tail-area probabilities for the NEX ensemble differ more, but our qualitative
104 results and conclusions hold.

105

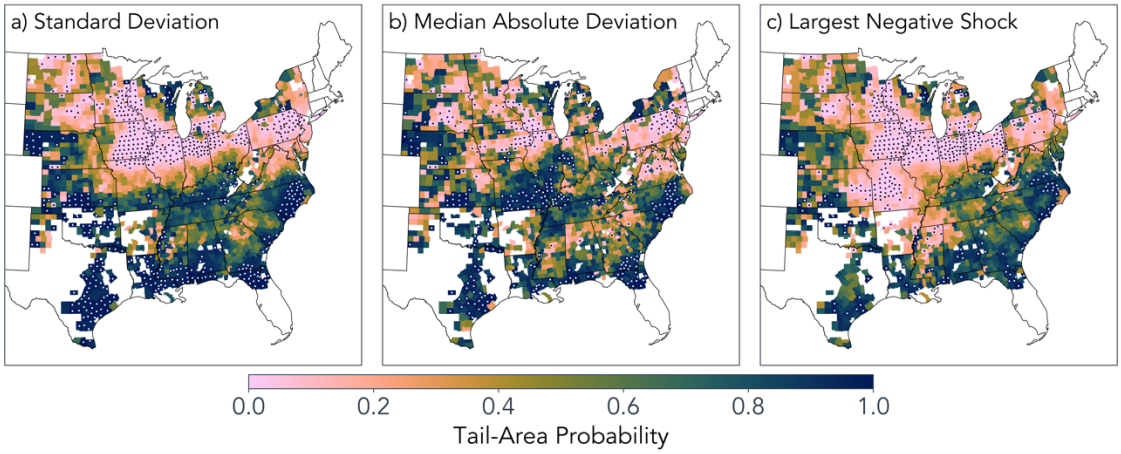

106

107 **Figure S8.** As Figure 2 in the main text but including all counties, regardless of whether including
108 climate variables increases skill.

109

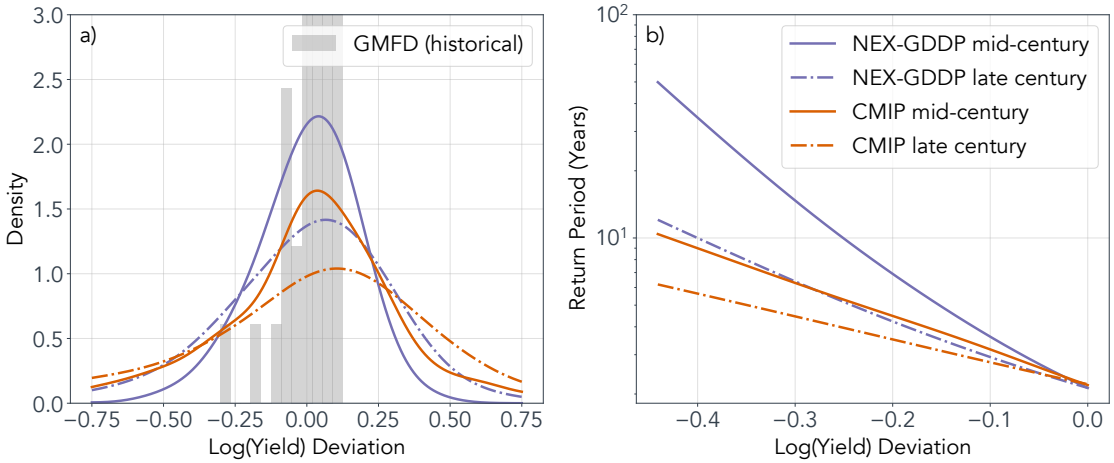

Figure S9. As Figure 4 in the main text but including all counties, regardless of whether including climate variables increases skill. The projected yield density functions are almost indistinguishable, as are the corresponding return periods.

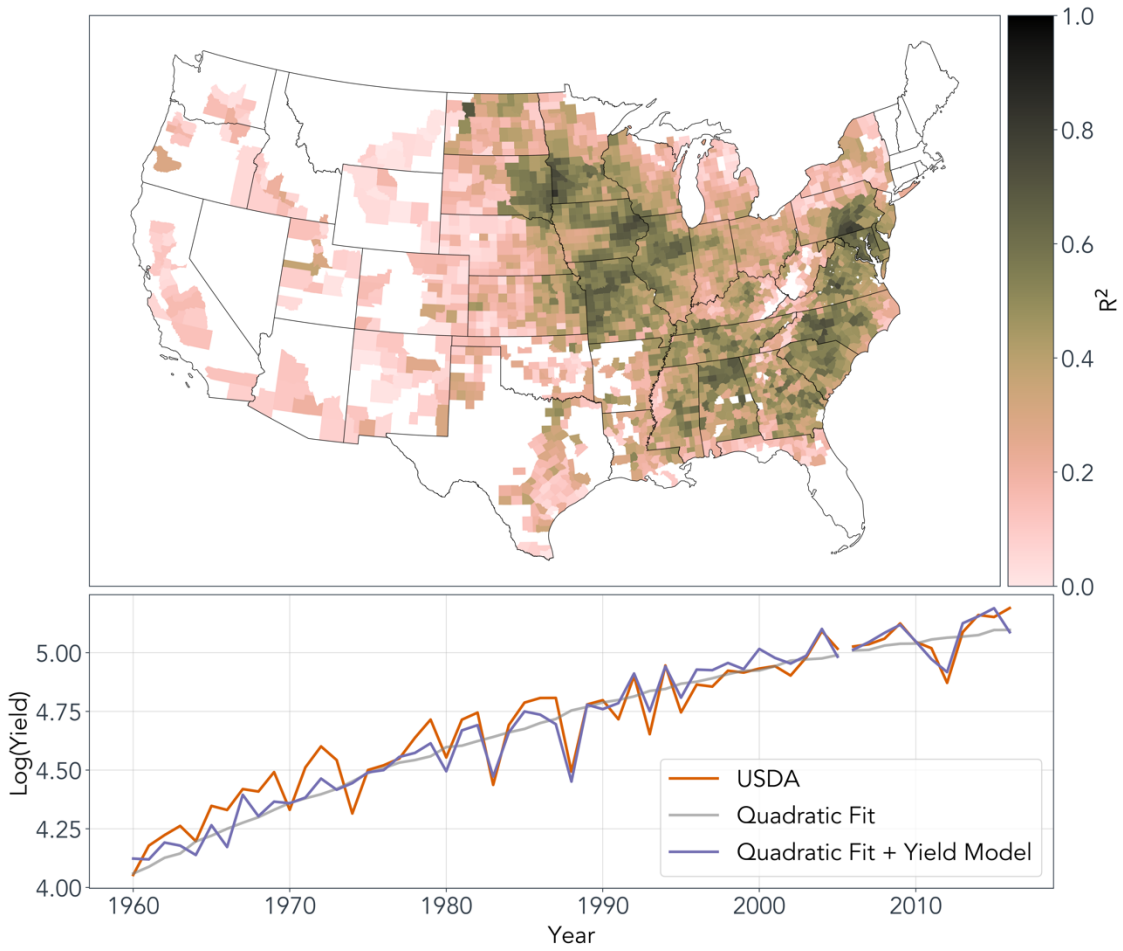

Fig. S10. (top) Yield model coefficient of determination measured against USDA records over the historical time period (1960-2005). Counties in white are those that exhibited less than 50% data coverage in the USDA record. (bottom) Annual national-level yield time series, constructed by summing county-level yields with weights equal to yearly historical production shares. The USDA record is shown in orange, the full yield model is shown in purple, and the time trend is shown in gray.

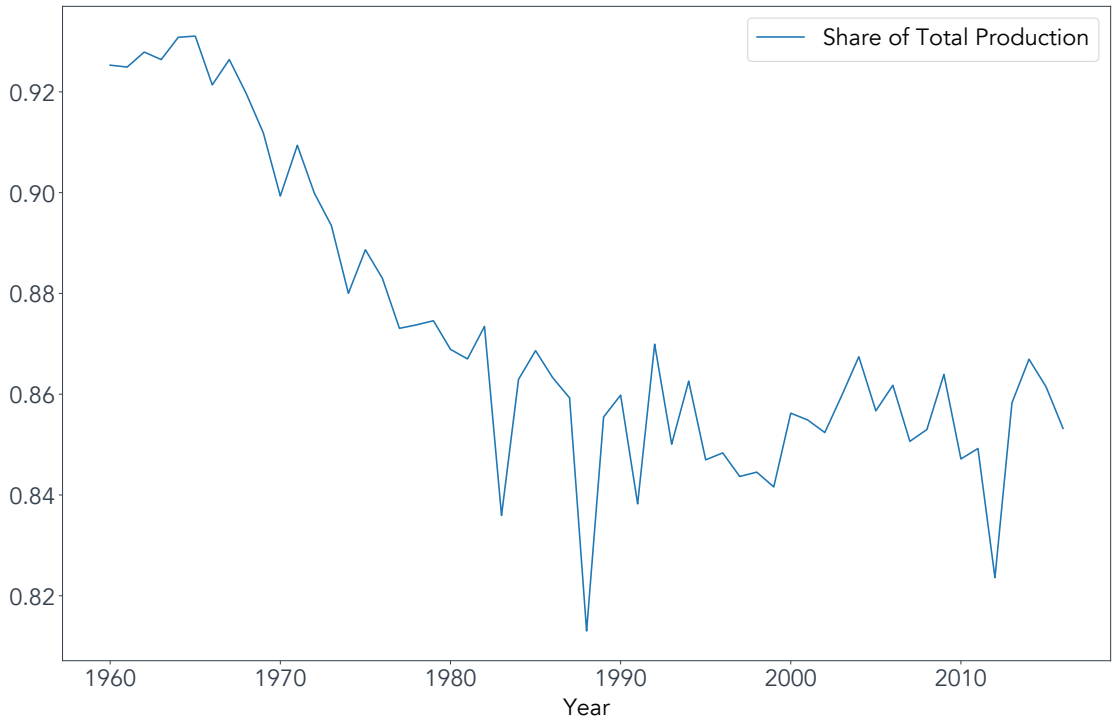

Figure S11. Summed production of counties for which including climatic variables in the yield model give an improved out-of-sample performance, measured relative to the total national level production each year.

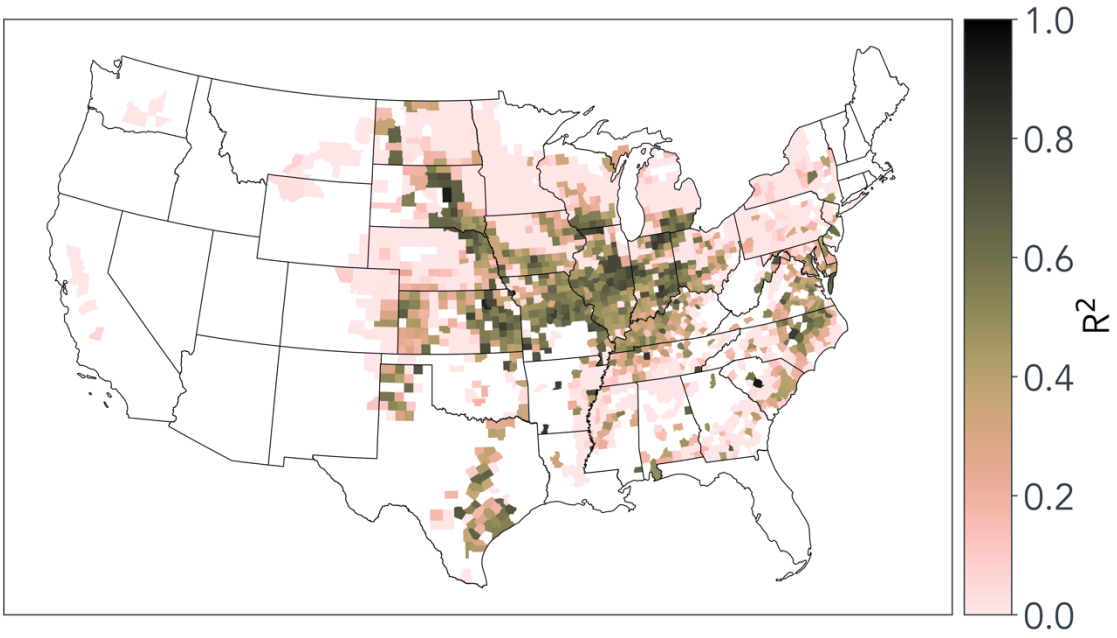

Figure S12. Coefficient of determination, R^2, for the out-of-sample period (2006-2016).

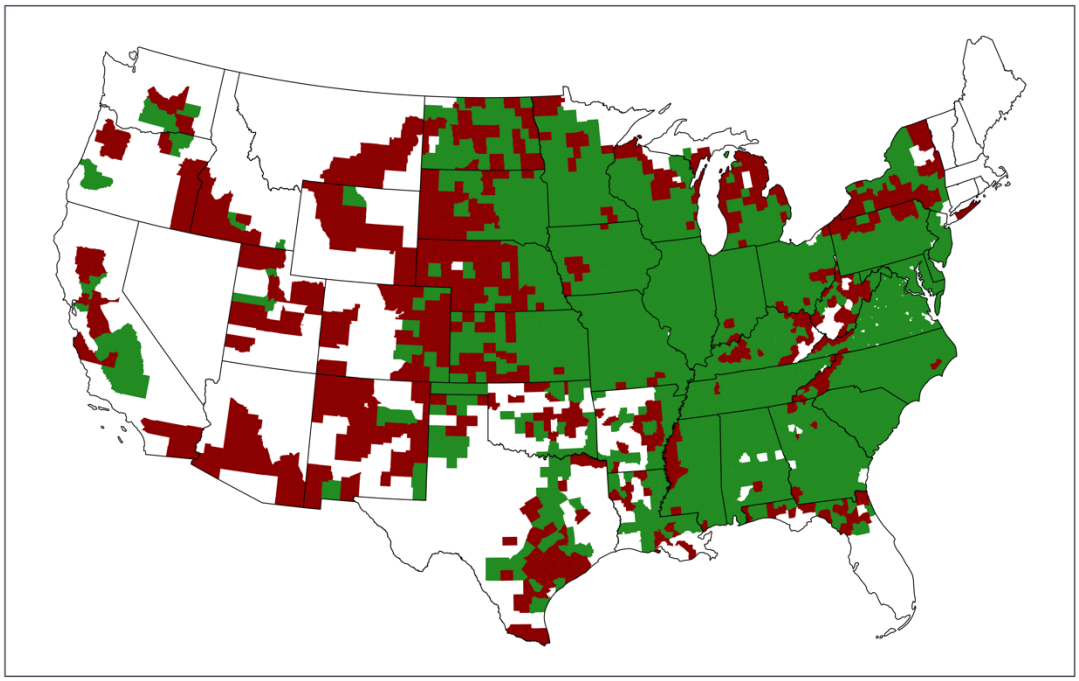

Figure S13. Counties for which including climatic variables in the yield model give an improved out-of-sample performance are shown in the green; those for which a worse fit is observed are shown in red.

140 **Table S1**. CMIP5 models and native resolutions
141

Model Name	Modeling Agency	Resolution (lat x lon)
ACCESS1-0	Commonwealth Scientific and Industrial Research Organization and Bureau of Meteorology, Australia	1.24° x 1.875°
BCC-CSM1-1	Beijing Climate Center, China Meteorological Administration	2.8125° x 2.8125°
BNU-ESM	College of Global Change and Earth System Science, Beijing Normal University, China	2.8125° x 2.8125°
CanESM2	Canadian Centre for Climate Modelling and Analysis, Canada	2.8125° x 2.8125°
CCSM4	National Center for Atmospheric Research, USA	0.9375° x 1.25°
CESM1-BGC	National Center for Atmospheric Research, USA	0.9375° x 1.25°
CNRM-CM5	National Centre of Meteorological Research, France	1.40625° x 1.40625°
CSIRO-MK3-6-0	Commonwealth Scientific and Industrial Research Organization & Queensland Climate Change Centre of Excellence, Australia	1.875° x 1.875°
GFDL-CM3	Geophysical Fluid and Atmospheric Administration Dynamics Laboratory, USA	2° x 2.5°
GFDL-ESM2G	Geophysical Fluid and Atmospheric Administration Dynamics Laboratory, USA	2° x 2.5°
GFDL-ESM2M	Geophysical Fluid and Atmospheric Administration Dynamics Laboratory, USA	2° x 2.5°
INMCM4	Institute for Numerical Mathematics, Russia	1.5° x 2°
IPSL-CM5A-LR	Institut Pierre-Simon Laplace, France	1.875° x 3.75°
IPSL-CM5A-MR	Institut Pierre-Simon Laplace, France	1.25° x 2.5°
MIROC-ESM	Japan Agency for Marine-Earth Science and Technology, Atmosphere and Ocean Research Institute (The University of Tokyo), and National Institute for Environmental Studies, Japan	2.8125° x 2.8125°
MIROC-ESM- CHEM	Japan Agency for Marine-Earth Science and Technology, Atmosphere and Ocean Research Institute (The University of Tokyo), and National Institute for Environmental Studies, Japan	2.8125° x 2.8125°
MIROC5	Atmosphere and Ocean Research Institute (The University of Tokyo), National Institute for Environmental Studies, and Japan Agency for Marine-Earth Science and Technology, Japan	1.40625° x 1.40625°
MPI-ESM-LR	Max Planck Institute for Meteorology, Germany	1.875° x 1.875°
MPI-ESM-MR	Max Planck Institute for Meteorology, Germany	2.875° x 1.875°
MRI-CGCM3	Meteorological Research Institute, Japan	1.125° x 1.125°
NorESM1-M	Norwegian Climate Centre, Norway	1.875° x 2.5°

References

1. Sheffield, J., Goteti, G. & Wood, E. F. Development of a 50-Year High-Resolution Global Dataset of Meteorological Forcings for Land Surface Modeling. *J Climate* **19**, 3088–3111 (2006).

2. Rosenzweig, C. *et al.* Assessing agricultural risks of climate change in the 21st century in a global gridded crop model intercomparison. *Proc National Acad Sci* **111**, 3268--3273 (2014).

3. Blanc, E. & Schlenker, W. The Use of Panel Models in Assessments of Climate Impacts on Agriculture. *Rev Env Econ Policy* **11**, 258–279 (2017).

4. Lobell, D. B. & Asseng, S. Comparing estimates of climate change impacts from process-based and statistical crop models. *Environ Res Lett* **12**, 015001 (2017).

5. Hoffman, A. L., Kemanian, A. R. & Forest, C. E. Analysis of climate signals in the crop yield record of sub-Saharan Africa. *Global Change Biol* **24**, 143–157 (2018).

6. Leng, G. & Hall, J. W. Predicting spatial and temporal variability in crop yields: an inter-comparison of machine learning, regression and process-based models. *Environ Res Lett* **15**, 044027 (2020).

7. Jeong, J. H. *et al.* Random Forests for Global and Regional Crop Yield Predictions. *Plos One* **11**, e0156571 (2016).

8. Crane-Droesch, A. Machine learning methods for crop yield prediction and climate change impact assessment in agriculture. *Environ Res Lett* **13**, 114003 (2018).

9. Schlenker, W. & Roberts, M. J. Nonlinear temperature effects indicate severe damages to U.S. crop yields under climate change. *Proc National Acad Sci* **106**, 15594 (2009).

10. Hsiang, S. *et al.* Estimating economic damage from climate change in the United States. *Science* **356**, 1362–1369 (2017).

11. Diffenbaugh, N. S., Hertel, T. W., Scherer, M. & Verma, M. Response of corn markets to climate volatility under alternative energy futures. *Nat Clim Change* **2**, 514–518 (2012).